The Energy Confinement response of DIII-D plasmas to Resonant Magnetic Perturbations

L. Cui[1], R. Nazikian[1], B.A. Grierson[1], E.A. Belli [2], T.E. Evans[2], N.C. Logan[1], D.M. Orlov[3], S.P. Smith[2], G. M. Staebler[2] and P. B. Snyder[2]

[1]Princeton Plasma Physics Laboratory, Princeton, New Jersey 08543, USA

[2]General Atomics, PO Box 85608, San Diego, California 92186-5608, USA

[3]University of California-San Diego, La Jolla, CA 92186, USA

Abstract

Resonant Magnetic Perturbations (RMPs) are a leading method for edge localized modes (ELMs) Control in fusion plasmas. However they can also cause a rapid degradation in energy confinement. In this paper we show that the energy confinement in low collisionality (ν_e^* < 0.3) DIII-D ITER Similar Shape (ISS) plasmas often recovers after several energy confinement times for RMP amplitudes up to the threshold for ELM suppression. Immediately following the application of the RMP, the plasma stored energy decreases in proportion to the decrease in the line-averaged density during density "pump-out". Later in the discharge confinement recovery is observed in the thermal ion channel and is correlated with the increase in the ion temperature at the top of the H-mode pedestal. A correlation between the inverse scale length of the ion temperature (a/L_{Ti}) and the $E \times B$ shearing rate at the top of the pedestal is seen during the confinement recovery phase. Transport analysis reveals that the confinement improvement in the ion channel results from the self-similarity in the ion temperature profiles in the plasma core combined with the observed increase in a/L_{Ti} in the plasma edge following density pump-out. In contrast the electron temperature scale length (a/L_{Te}) remains essentially unchanged in response to the application of the RMP. At significantly higher RMP levels the edge $E \times B$ shearing rate and a/L_{Ti} does not increase and the confinement does not recover following density pump-out.

I. Introduction and Motivation

Future fusion reactors must control the divertor heat flux due to Edge Localized Mode (ELMs) in order to preserve the lifetime of plasma facing components and to prevent eroded material from penetrating the plasma and possibly terminating the discharge [1]. One method to control these instabilities is by the use of Resonant Magnetic Perturbations (RMPs) [2].

In low collisionality plasmas the universal observation is that the application of the RMP leads to a drop in the plasma density and stored energy. This drop in density is called density pump-out [3]. Impurity transport is also increased with RMP, which is beneficial for future reactors [4]. It is an important goal to minimize the stored energy reduction in RMP plasmas in order to optimize fusion performance while effectively removing He ash and impurities.

In the DIII-D RMP experiments with ITER Similar Shape (ISS) [3] plasmas using n=3 RMPs, we observe a surprising recovery in the plasma stored energy on longer time scales (several global energy confinement time τ_E) following the initial reduction in τ_E during density pump-out without a recovery in the particle confinement. We find that the energy confinement can fully recover in DIII-D plasmas for modest levels of RMP amplitude (here the RMP amplitude refers to the vacuum magnetic perturbation of the n = 3 field at the plasma surface that 1 kA RMP coil current produces $\delta b_r^{(m,n)} B_T^{-1} \sim 0.8\times10^{-4}$ with m = 10 and n=3) slightly above the threshold for ELM suppression. For RMP level well above the ELM suppression threshold, the energy confinement does not recover to the pre-RMP level. Understanding this phenomenon of confinement recovery for moderate RMP amplitudes is essential to having confidence in achieving ELM suppression without degradation of the stored energy.

Application of the I-coil current leads to a transient phase of the plasma discharge characterized by density pump-out. ELM suppression can result from a sufficiently large I-coil current. Generally, under good wall conditions (when the walls are not outgassing excessively) and with optimal pumping, ELM

suppression can be achieved with coil currents as low as 2.0 kA, the applied resonant field at the m/n=10/3 surface (the vacuum field) $\delta b_r^{(10,3)} B_T^{-1}$ ~ 1.8×10^{-4} in the ISS shape with n=3 RMP fields and for pedestal electron collisionality ν_e^* <0.3 [3]. Fig. 1 shows a typical example of a discharge where the RMP is at the threshold for ELM suppression. Plasma parameters for these experiments are: B_T=1.96T, I_p=1.6 MA, q_{95}~3.5, normalized beta $\beta_N = \beta/(I_p/aB_T)$ varies from β_N=1.6 to β_N=2, P_{inj} ~6 MW, T_{inj}~ 5Nm, plasma total stored energy W_{MHD} ~0.95-1.15 MJ, line-averaged density n_e=3.5×10^{19}- 4.5×10^{19} m^{-3}. There is a prompt reduction in total stored energy W_{MHD} and line-averaged density in the first 150 ms (≈1 τ_E) of the RMP that is referred as the "pump-out phase" in this paper. Later W_{MHD} recovers to the pre-RMP level within $3\tau_E$, which is referred to as the "recovery phase" without any recovery in the electron density. Most of the confinement recovery takes place before the transition to ELM suppression at t ~3.0 s [Fig. 1(c)], even though the line-averaged density continues to decay over the entire period up to ELM suppression. When the plasma enters into ELM suppression the confinement experiences a further increase, possibly resulting from the cessation of ELM induced losses and possibly from the small increase in the line density.

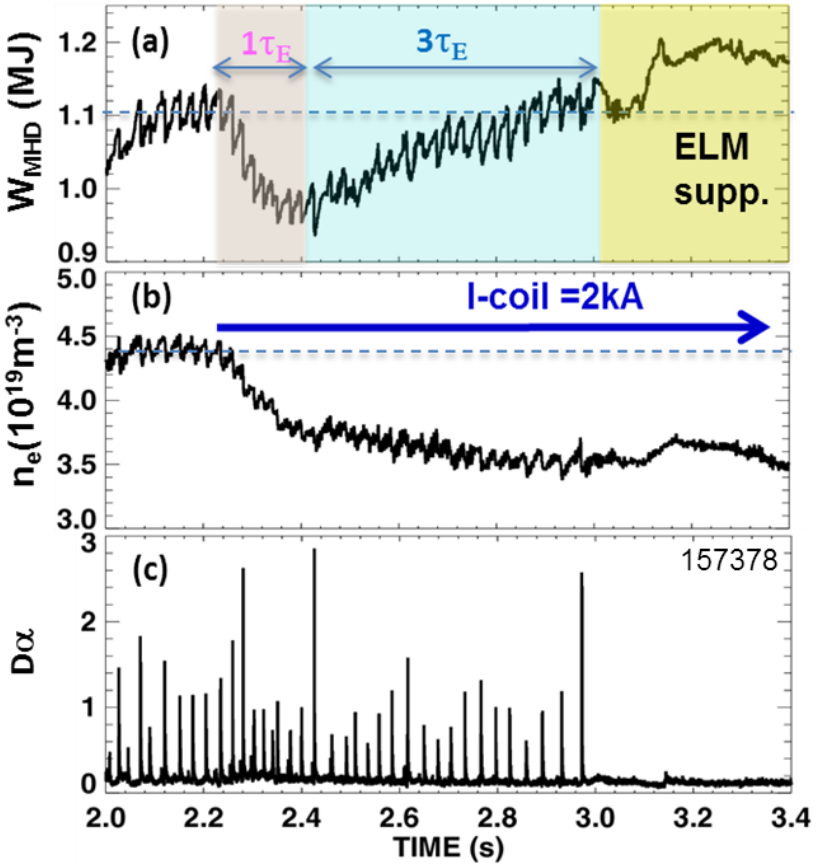

Figure 1 A discharge with n=3 RMP shows: (a) total stored energy $\boldsymbol{W_{MHD}}$, (b) line-averaged density, (c) $\boldsymbol{D_\alpha}$. With $\boldsymbol{P_{inj}}$ ≈ 6 MW, beam torque ≈ 5 Nm. Shot 157378.

In this paper, we focus primarily on the energy confinement recovery of plasmas following density pump-out during the ELMing phase of the discharge. We look specifically at the dynamics of the confinement recovery and assess the causes for this recovery based on transport model analysis and measured pedestal parameters. From Fig. 1 we see that the dominant effect on the confinement recovery does not come during ELM suppression but rather during the ELMing phase following density pump-out. We note that the rate of energy loss due to ELMs is almost constant in both the pre RMP phase and in the confinement recovery phase, which indicates that the confinement improvement cannot be attributed to a reduction in the rate of ELM induced energy loss. At much higher RMP amplitudes $\boldsymbol{\delta b_r^{(10,3)} B_T^{-1}} \sim 4.4\times10^{-4}$), with an

RMP current of 5 kA, we observe a significant and sustained degradation of confinement without any obvious sign of recovery (see section IV).

The relative insensitivity of the confinement to the RMP level and density pump-out on a long time scale is the key topic that we investigate in this paper. We show from profile and transport code (TRANSP [5]) analysis that the overall favorable confinement performance of these plasmas on long time scales arises from an improvement in the ion thermal channel. The improved ion thermal confinement is evident from a global increase in the ion temperature following density pump-out and arises from a combination of an increase of the ion temperature inverse scale length (a/L_{Ti}) in the pedestal with ion temperature profile self-similarity in the core. Furthermore, analysis reveals that the increase in a/L_{Ti} in the pedestal is correlated with the increase in the $E \times B$ shearing rate in the same region, whereas plasmas that do not show improved confinement have a stationary or decreasing edge E×B shearing rate. In this paper we will not address the confinement changes in ELM suppression. Rather we restrict ourselves to the confinement improvement observed during the ELMing phase of the discharge with the RMP prior to the onset of suppression.

The outline of this paper is as follows. In section II, we will present experimental observations of confinement recovery and the edge pedestal response. In section III, transport analysis indicates the key role played by the edge $\boldsymbol{a/L_{Ti}}$ in the confinement recovery. In section IV, we extend the discussion to high RMP amplitudes where confinement does not recover following density pump-out and where no increase is seen in the pedestal E×B shearing rate. This is consistent with the picture presented above where the confinement improvement arises from an increase in the edge $\boldsymbol{a/L_{Ti}}$ due to an increase in the edge E×B shearing rate. In section V, we summarize these results and indicate next steps in the research.

II. Experimental results

Experiments were conducted in the ITER Similar Shape (ISS) plasmas on DIII-D to address the effects of n=3 Resonant Magnetic Perturbations (RMPs) on pedestal transport and global confinement. The

experiments were performed using the DIII-D Internal Coils (I-coils [6]) in an even parity n=3 configuration. The DIII-D I-coils consist of two rows of six upper and six lower coils, capable of producing a strong n=3 harmonic. Even parity means that the upper and lower coil currents are in phase. The I-coil current ranged from 1 kA to 6 kA in these experiments, producing a vacuum magnetic perturbation at the plasma surface $\delta b_r^{(10,3)} B_T^{-1} \sim$ 0.8 – 4.8×10^{-4}. This configuration is optimal for achieving ELM suppression in a finite window of edge magnetic safety factor $q_{95} \approx 3.5$. A cross section of the plasma equilibrium is provided in Fig. 2 showing the proximity of the I-coils to the plasma boundary and the lower single null configuration of the plasma with the outer strike point at the optimal location for particle pumping.

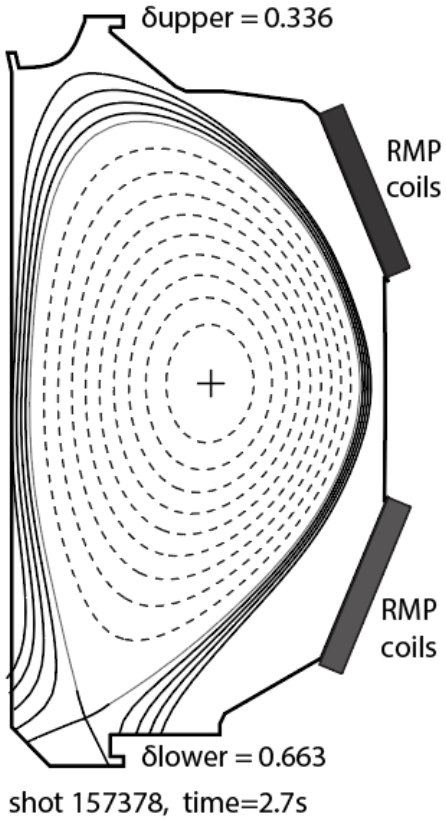

Figure 2 Equilibrium cross-section and the location of the I-coils for ISS RMP H-mode experiments (shot 157378 at 2700 ms.)

In these experiments, the degree of density pump-out is sensitive to the level of the applied RMP while on a long time scale the confinement recovery is relatively insensitive to the RMP level around the threshold of ELM suppression. In Fig. 3, we show four discharges with different levels of I-coil current (1 kA, 1.7 kA, 2 kA and 2.5 kA) with different levels of density pump-out. The discharges are well matched in density and plasma stored energy at the start of the RMP and all discharges have the same beam power (≈ 6 MW) and beam torque (≈ 5 Nm). I-coils are applied near t =2.24s and a rapid drop (pump-out phase) is seen in the stored energy and line-average density in response to the RMP. On a longer time scale (recovery phase), the density stays reduced, while the stored energy for all four discharges starts to rise and approaches the pre-RMP level. We note that during this early discharge phase, current profiles are slowly evolving that could associate with a contribution to the increase in confinement. It is already known that 1 kA RMP coil current has little effect on DIII-D plasmas, which can be taken as an estimate for non-RMP case that shows the increment of stored energy during this time region (t~ 2.24s -3.2s) is much smaller than the increment in the other three higher RMP cases. Therefore, the recovery of stored energy related to RMP effect plays a dominant role in this time region. As the beam power is constant, the confinement trend simply follows the trend in the stored energy. The total absorbed power is a combination of 6 MW of 80 keV deuterium beams and 1 MW of additional heating from the Ohmic current. At t ~ 3.2s, the stored energy in all four discharges is nearly equal even though the level of density pump-out is different for each of the discharges. Note that two of the four discharges eventually experience ELM suppression because the threshold for ELM suppression in these ISS plasmas is close to 2 kA of I-coil current.

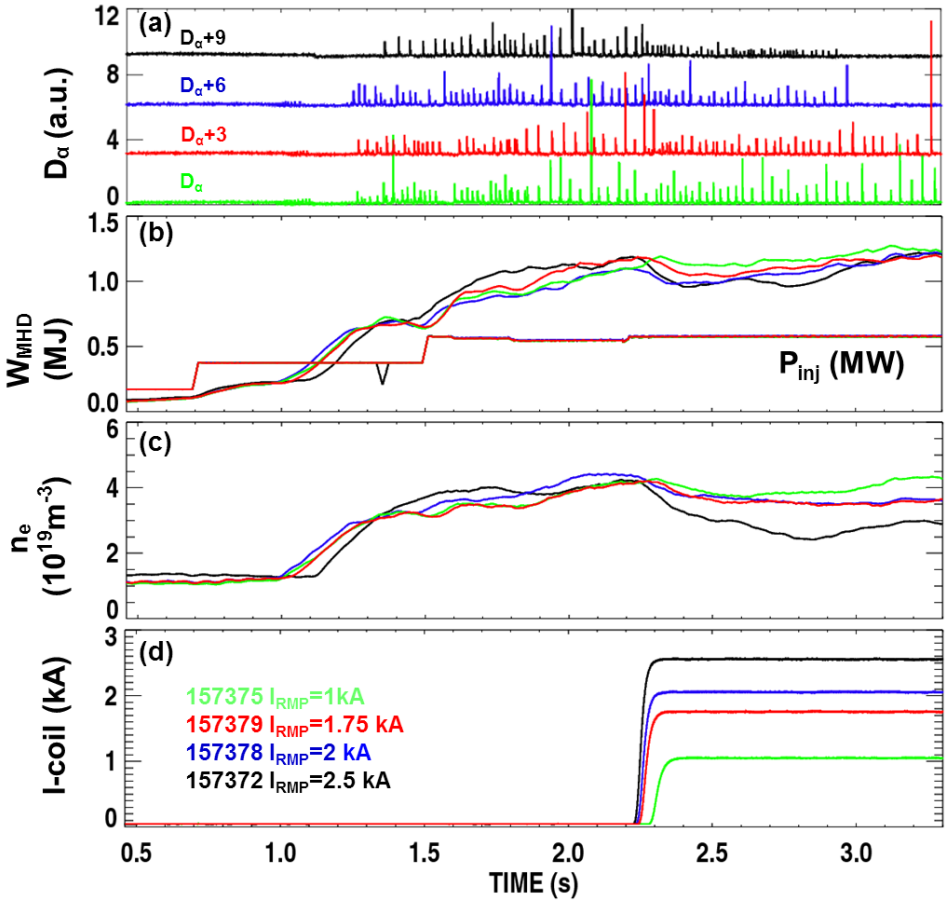

Figure 3 Comparison of discharges with similar beam power $\mathbf{P_{inj}}$≈6MW and $\mathbf{q_{95}}$~3.5 but different I-coil currents, 1 kA, 1.7 kA 2 kA, 2.5 kA. (a) $\mathbf{D_\alpha}$, (b) $\boldsymbol{W_{MHD}}$ and $\mathbf{P_{inj}}$, (c) line-average density and (d) I-coil current.

Inspection of the early phase of the RMP after 2.2 s shows that the level of reduction in the plasma stored energy and line-averaged density increase with I-coil current. Fig. 4 shows the time evolution of the stored energy, line-averaged density and I-coil current in the early phase of two discharges from Fig. 3 with applied RMP. Assuming that the neutral fueling in the core is not decreasing rapidly in the early phase of the RMP, the data indicates a strong degradation in the global particle confinement with increasing RMP amplitude. This is consistent with impurity transport measurements that show a strong decrease in low-Z and intermediate-Z impurity confinement time with increasing RMP level [4].

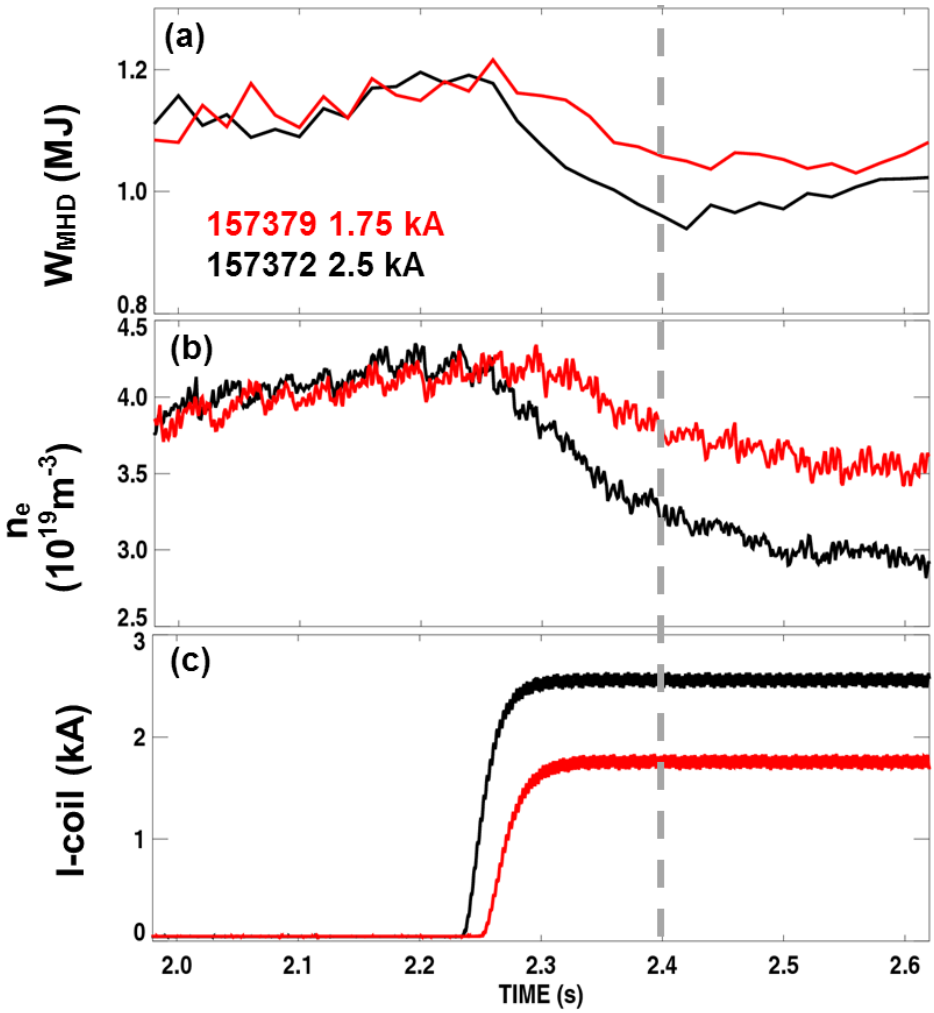

Figure 4 The time evolution at early phase of the applied RMP for: (a) total stored energy, (b) line-averaged density and (c) I-coil current.

A detailed look at the pump-out phase of these discharges also shows that the plasma stored energy stops decaying before the density pump-out is complete. We see in Fig. 4 that the line-averaged density continues to decrease when the stored energy reaches its minimum at t~2.4 s and then the stored energy begins to level off and even improve while the line-averaged density is still decreasing rapidly in the pump-out phase. At t~2.4 s, the percentage drop in the stored energy is close to the percentage drop in the line-averaged density, corresponding to ~ 12 % and 20% for I-coil current of 1.75 kA and 2.5 kA, respectively. From this result we can determine that the plasma confinement improvement begins early in the density pump-out phase ~100 ms following the RMP turn on.

Next we show that there is a trend of increasing in the ion temperature at the top of pedestal (in this paper also refers to edge T_i) during the confinement recovery phase and to a lesser extent an increase in the electron temperature. Fig. 5 shows the evolution of electron density and temperature as well as carbon toroidal rotation at the top of the pedestal for discharge 157378 with 2 kA of I-coil current. This evolution is illustrative of the behavior of other discharges in this data set, at least for I-coil currents up to the threshold of ELM suppression (~2 kA). The pedestal electron density and temperature come from Thomson scattering measurements while the ion temperature and toroidal rotation are measured from carbon C-VI using Charge Exchange Recombination (CER) spectroscopy. We note that in the recovery phase the stored energy is correlated with the strong increase of the edge ion temperature beginning during the early phase of the density pump-out and continuing late into the discharge. From the start of the RMP (t ~ 2.24s) to 2.9s, there are significant changes at the top of pedestal (shown at ρ ~ 0.9): the ion temperature increases by ≈ 30% while the electron temperature increases by ≈ 10% and the electron density decreases by ≈ 33%. In Fig. 5(c), we show the measured toroidal rotation velocity V_{tor} at two different radial locations during the recovery phase: one is at ρ ~ 0.9 and the other is at the separatrix. There is a significant increase of V_{tor} at top of pedestal while the value at separatrix slightly increases, which suggests an increase in the toroidal rotation shear in the pedestal region.

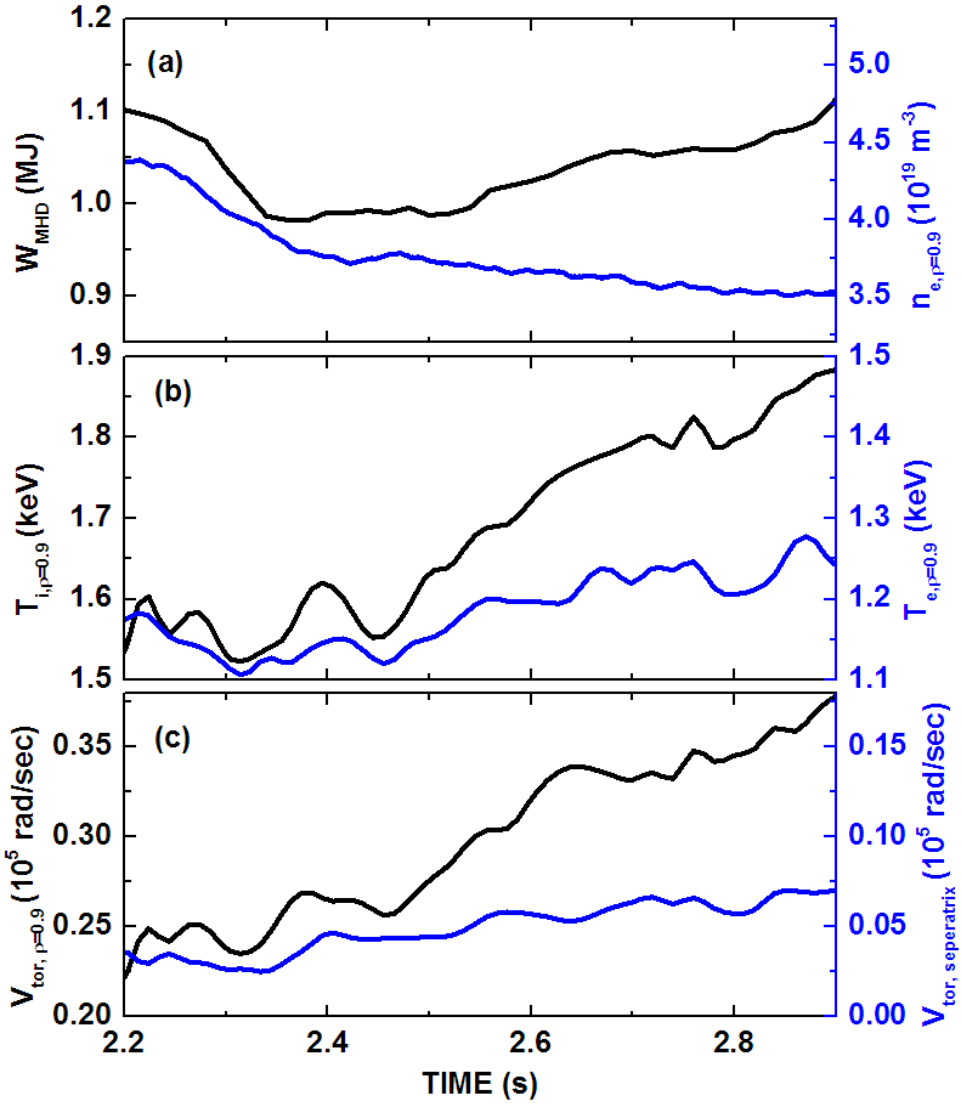

Figure 5 The time-evolution for quantities at $\boldsymbol{\rho}$ = 0.9 (top of pedestal) with I-coil current=2 kA: (a) electron density from Thomson scattering data at $\boldsymbol{\rho}$ = 0.9 (blue) and stored energy (black), (b) ion temperature from CER data (black) and electron temperature from Thomson scattering data (blue) at $\boldsymbol{\rho}$ = 0.9, (c) toroidal rotation from CER data at $\boldsymbol{\rho}$ =0.9 (black) and at separatrix (blue). Shot #157378.

Here, we show that the reduction in the stored energy in the early phase of the RMP matches fairly well the reduction in the pedestal density whereas the recovery of the stored energy following pump-out matches fairly well the increase in the edge ion temperature. From the four discharges with different I-coil currents shown in Fig. 3, we compute the percentage changes in the plasma stored energy, line-averaged

density, edge density and edge ion temperature versus RMP amplitude. Every data point is the time average of a 100 ms time window. Fig. 6(a) shows the changes in the early RMP phase from 2.2s-2.4s during the pump-out phase. Both the line-averaged density and edge density decrease with the application of RMP, and the percentage of change is proportional to the amplitude of the RMP I-coil current. The pump out is much stronger in the plasma edge than the plasma core, as revealed by the edge pedestal density decrease relative to the line-averaged density decrease. The percentage decrease in the plasma stored energy is close to the percentage decrease in the line-averaged density. Fig. 6(b) shows the changes in the stored energy and ion temperature at ρ ~ 0.9 ($T_{i,0.9}$) versus I-coil current for the same discharges during the recovery phase from 2.4 to 2.8 s. It is evident that the recovery of the stored energy is proportional to the increase in the edge ion temperature in these plasmas. This suggests that the confinement improvement is closely tied to ion thermal transport.

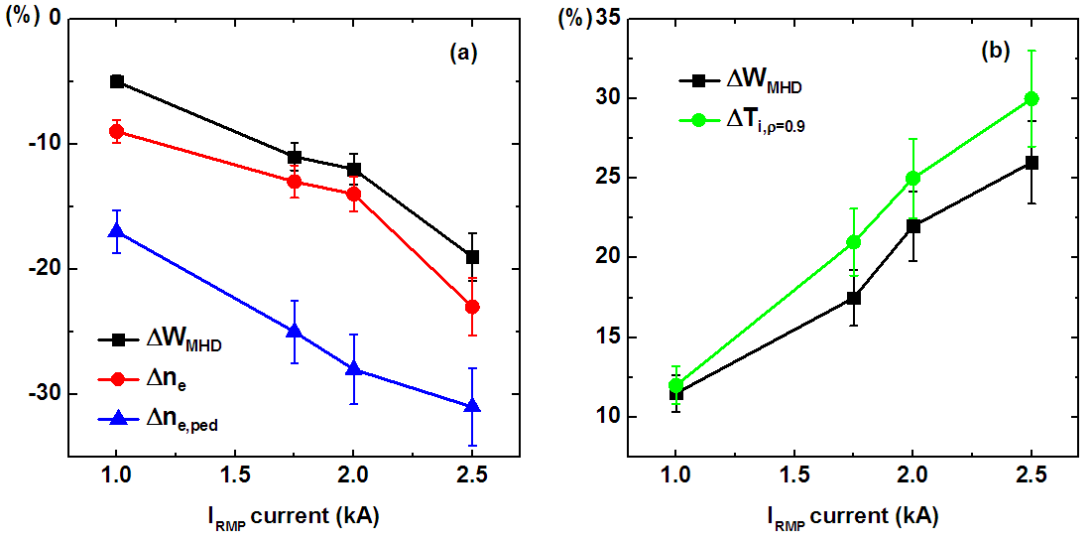

Figure 6 (a) The percentage decrease in stored energy (black), percentage decreases in line-averaged pedestal (red) and percentage decreases in pedestal density (blue) vs I-coil current at the minimum of the stored energy compared to just before the I-coil current turns on; (b) The percentage increase in stored

energy (black) and percentage increases in $\boldsymbol{T_{i,\rho=0.9}}$ (green) in the recovery phase compared to the time of minimum stored energy. The I-coil currents of 1 kA, 1.75 kA, 2 kA and 2.5 kA, correspond to discharges 157375, 157379, 157378 and 157372 respectively.

Profile analysis is performed using the One Modeling Framework for Integrated Tasks (OMFIT) [7]. Radial profiles of density, electron and ion temperature vs ρ (sqrt. of normalized toroidal flux) are shown in Fig. 7 for shot 157378. We display profiles at three times of interest corresponding to the pre-RMP, pump-out, and recovery phase, at t = 2.2, 2.4 and 2.8 s, respectively. In Fig. 7(a-c) profiles are shown for the pre-RMP and pump-out phase. In Fig. 7(d-f) profiles are shown for the pump-out and recovery phase. As we can see in the pump-out phase, there is little change in the $\boldsymbol{T_e}$ and $\boldsymbol{T_i}$ profile from 2.2 to 2.4 s. The main reduction is in the electron density primarily at the plasma edge. However, from 2.4 to 2.8 s, we see a significant increase in the core $\boldsymbol{T_i}$ by ~ 12% whereas the core $\boldsymbol{T_e}$ increases by only ~ 5%. There is a continuous though weak decrease in the edge electron density on the longer time scale. From these profile changes, it is evident that the recovery of the stored energy comes from a substantial increase in the core ion temperature offsetting the effect of the density reduction.

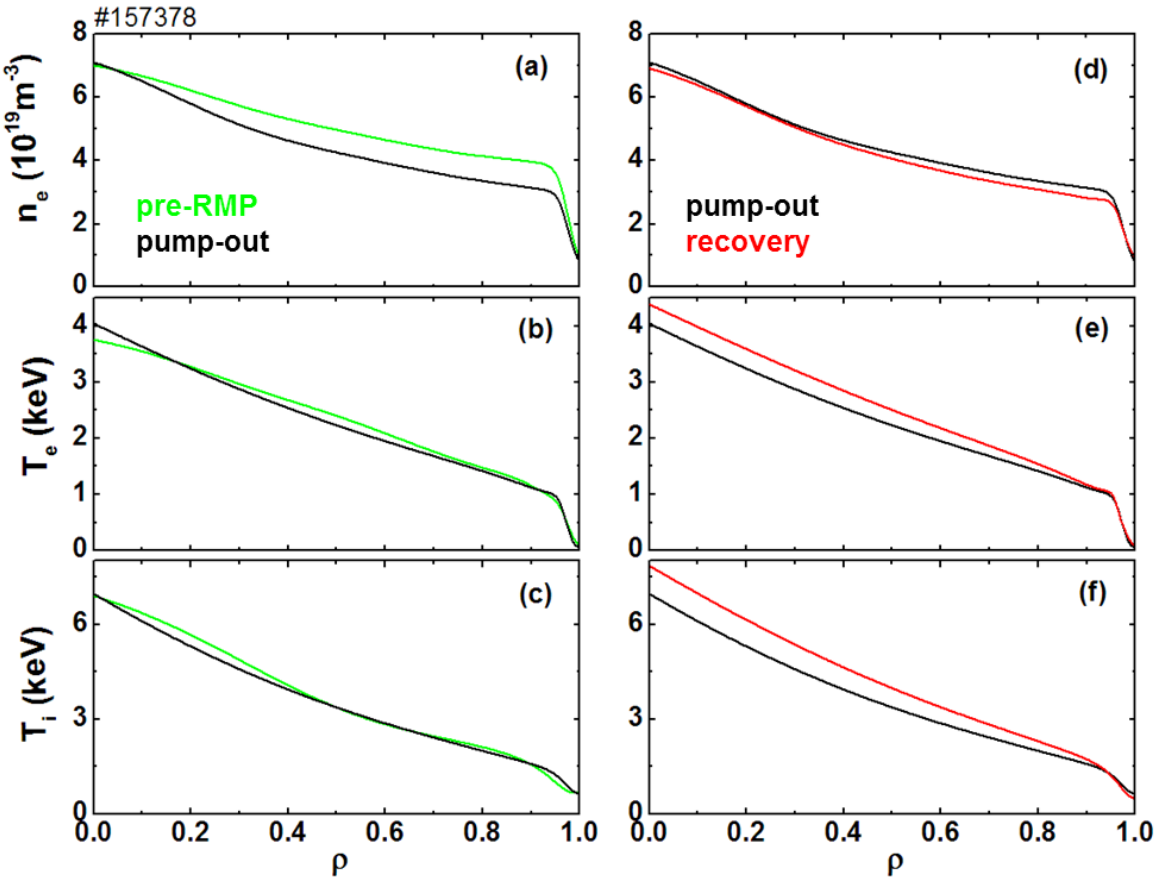

Figure 7 Comparison of measured profiles for the pump-out phase (shown in black) and pre-RMP (shown in green) phase: (a) electron density $\boldsymbol{n_e}$, (b) electron temperature $\boldsymbol{T_e}$ and (c) ion temperature $\boldsymbol{T_i}$. Comparison of measured profiles for the pump-out phase and recovery phase (shown in red) are shown in (d-f).

Fig. 8 shows a close up view of the pedestal profiles at the minimum of the stored energy at t=2.4 s and later during recovery at t=2.8 s. Fig. 8 (a) shows that the edge electron temperature slightly increases during the energy confinement recovery phase at the top of pedestal. However, there is a more distinct increase in the T_i from ρ =0.8-0.9 as shown in Fig. 8(b). The inverse scale length of the edge T_e and T_i profiles are shown in Fig. 8(c-d). The increase in T_i at ρ =0.8 is predominantly arising from an increase in

a/L_{Ti} from ρ >0.9 with the largest change in a/L_{Ti} occurring close to the top of the pedestal at $\rho \approx 0.93$. In contrast, there is almost no change in the inverse scale length of T_e in this interval [8].

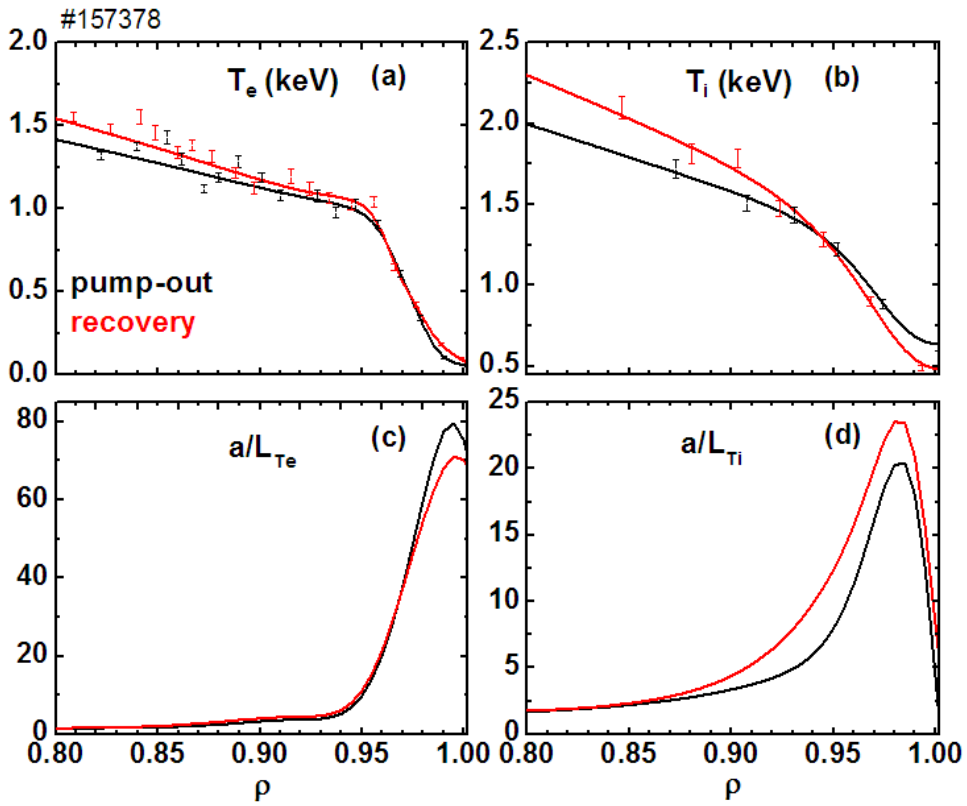

Figure 8 Edge radial profiles of (a) electron temperature (b) ion temperature, (c) inversed electron temperature scale length $\boldsymbol{a/L_{Te}}$ and (d) inversed ion temperature scale length $\boldsymbol{a/L_{Ti}}$ at t=2.4s (pump-out phase) and t=2.8s (recovery phase) for shot 157378.

The distinct change in the edge a/L_{Ti} indicates that a change in the edge ion thermal transport has occurred during the stored energy recovery. By taking an approximation of $E \times B$ shear frequency $\omega_{E\times B}$ from Waltz-Miller calculation [9], it is found to be of order $\frac{\partial E_r}{\partial \rho}$ that includes the contribution from the pressure gradient, toroidal rotation gradient and poloidal rotation gradient. By normalizing $\omega_{E\times B}$ with $\frac{C_s}{a}$ where a is the minor radius and C_s is the sound speed at the reference radius, we obtain the $E \times B$ shearing rate $\gamma_{E\times B}$. As we see in Fig. 9, in the top of the pedestal region the major contribution to $\gamma_{E\times B}$

comes from the toroidal rotation gradient that shows a similar increase with the $\gamma_{E\times B}$. This is consistent with the observation in Fig. 5(c). Figure 10(a) shows the trend in a/L_{Ti} with $\gamma_{E\times B}$ at ρ=0.93 during the recovery phase from 2.4 to 2.8 s. Fig. 10(b) shows the Ion Temperature Gradient (ITG) linear growth rate γ_{ITG} normalized by $\frac{c_s}{a}$ at kρ_s ~0.3 calculated by TGLF compared to the normalized E×B shearing rate $\gamma_{E\times B}$ at t=2.8 s. We see that γ_{ITG} is comparable to but somewhat larger than the $\gamma_{E\times B}$ across the top of the pedestal and the net growth rate $\gamma_{net} = \gamma_{ITG} - \gamma_{E\times B}$ is significantly reduced compared to the linear growth rate, which suggest that the increase in $E \times B$ shear is reducing turbulent transport [10]. Experimental measurements of density fluctuation at top of pedestal confirm the reduction of turbulence with the increasing $E \times B$ shear.

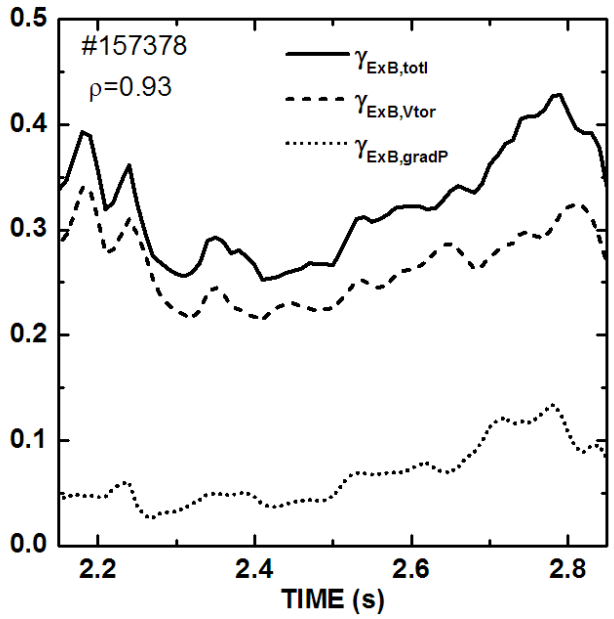

Figure 9 Contribution from pressure gradient (dotted line) and toroidal rotation gradient (dashed line) to E×B shearing rate at ρ=0.93.

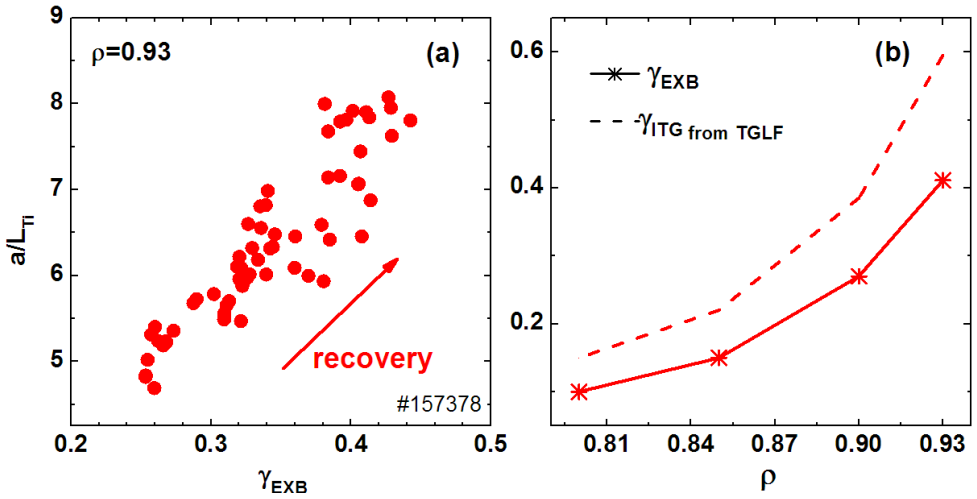

Figure 10 For shot #157378 (a) Correlation between $\boldsymbol{a/L_{Ti}}$ and $\boldsymbol{E \times B}$ shearing rate at $\boldsymbol{\rho}$=0.93 from t=2.4 s to 2.8 s. (b) Normalized ITG linear growth rate $\boldsymbol{\gamma_{ITG}}$ (dashed) versus normalized $\boldsymbol{E \times B}$ shearing rate $\boldsymbol{\gamma_{E\times B}}$ (in unit of $\frac{C_s}{a}$) at t=2.8 s calculated by TGLF.

The increase of E×B shearing rate appears to play a role in the increase of the edge T_i during recovery. It is interesting to see under what conditions the edge $E \times B$ shearing rate and a/L_{Ti} are correlated with confinement recovery. In Fig. 11 we compare 157378 with another discharge 158071 for which there is no confinement recovery, but with all other conditions identical to 157378. There is a higher pedestal density in 158071 that comes from poorer wall conditions in the discharge due to the use of deuterium gas puffs during that run day. The pedestal density in the plasma where W_{MHD} does not recover is about 25% - 35% higher than in the plasma where W_{MHD} recovers and the pedestal density does not exhibit a sustained reduction compared to the recovery discharge, neither does the stored energy. Fig. 11 (c) shows the ion temperature at large radii (ρ=0.9) is not increasing in the late RMP phase for the discharge where the stored energy does not recover, which correlates with a constant $E \times B$ shearing rate at the top of the pedestal in discharge 158071 compared to an increasing $E \times B$ shearing rate in discharge 157378 as shown in Fig. 11 (d).

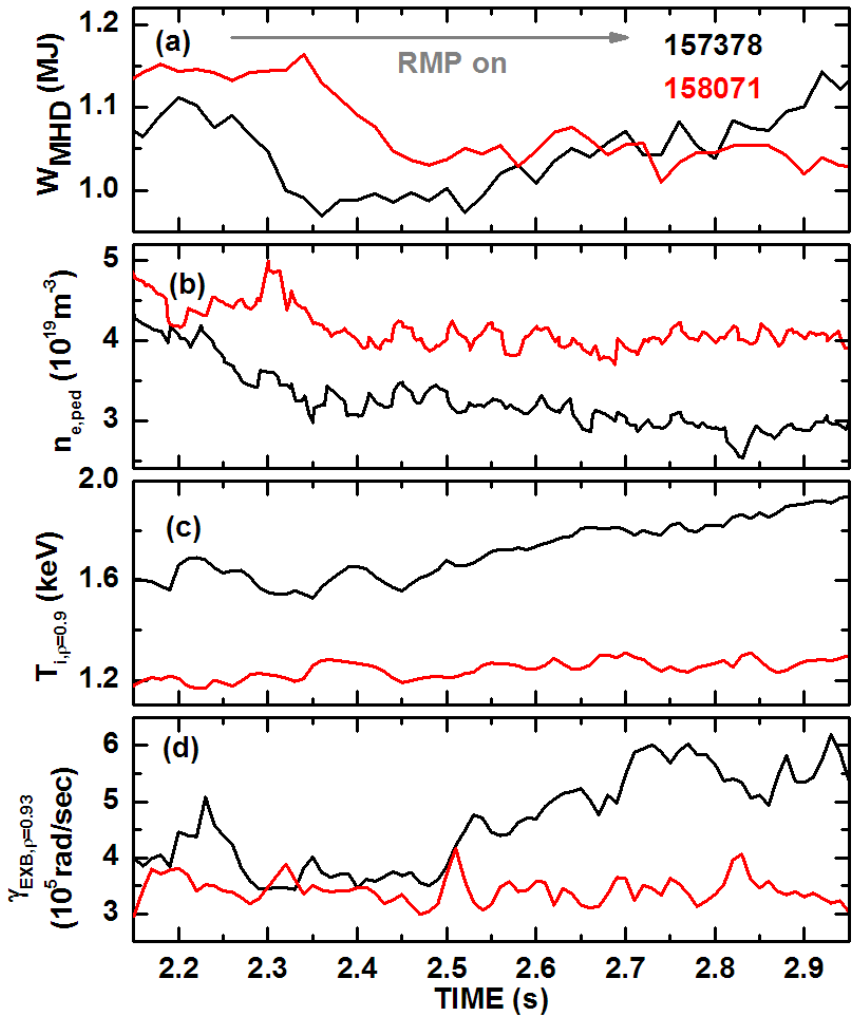

Figure 11 Comparison between two discharges with same RMP coil current (2kA), P_{inj} (6MW) and torque input (5 Nm). (a) plasma stored energy (b) pedestal electron density, (c) ion temperature at ρ=0.9 and (d) $E \times B$ shearing rate at ρ=0.93.

The comparison between two discharges with the same I-coil current in Fig. 11 indicates a correlation between the edge T_i and energy confinement recovery. It also suggests that the energy confinement recovery requires low electron pedestal density. To further investigate the correlation of the edge T_i and pedestal density $n_{e,ped}$ with respect to the confinement recovery, we extend our analysis to discharges with different I-coil currents and different pedestal densities. Fig. 12(a) shows the variation of the edge T_i

(here shows $T_{i,\rho=0.9}$) and $n_{e,ped}$ for a set of discharges with different I-coil current (< 2.5 kA). Each data point corresponds to a time during the confinement recovery phase. Time advances from the lower right to the top left for each discharge denoted by a different color symbol. A trend of increasing $T_{i,\rho=0.9}$ with decreasing pedestal density is evident for each I-coil current. Another observation is that for higher I-coil current the edge T_i is generally lower for a given pedestal density. However, we can also see that the edge T_i rises to higher values than for discharges with lower I-coil current. At the end of the recovery phase, the stored energy of the four discharges are approximately equal with W_{MHD}≈1.05 MJ, indicated by the diagonal dashed line in Fig. 12(a). The figure shows that the point of constant stored plasma energy corresponds to higher increasing edge T_i and decreasing $n_{e,ped}$ as the I-coil current increases.

In these discharges with fixed heating and beam torque, the dominant contribution to the $E \times B$ shearing rate comes from the toroidal rotation. To understand the connection between the toroidal rotation and the edge ion temperature we plot the differential toroidal velocity between ρ =0.9 and ρ =1.0 vs T_i at ρ =0.9 for the four discharges as shown in Fig. 12(b). Fig. 12(b) indicates that the differential toroidal rotation dV_{tor} and the ion temperature at the top of the pedestal are highly correlated in these plasmas. At lower I-coil current, the peak $T_{i,\rho=0.9}$ and dV_{tor} are lower, corresponding to the higher pedestal density from Fig. 12(a). For higher I-coil current, the dV_{tor} and the edge ion temperature are both higher, corresponding to the lower pedestal density. The correlation of the $E \times B$ shearing rate with a/L_{Ti} is consistent with the paradigm of long wavelength drift wave transport suppression by toroidal velocity shear. However, the trigger for such an evolution in the confinement recovery phase and its relation to edge density is not explored in this paper. In what follows we will show that the confinement recovery is consistent with the increase in the edge T_i according to reduced transport models.

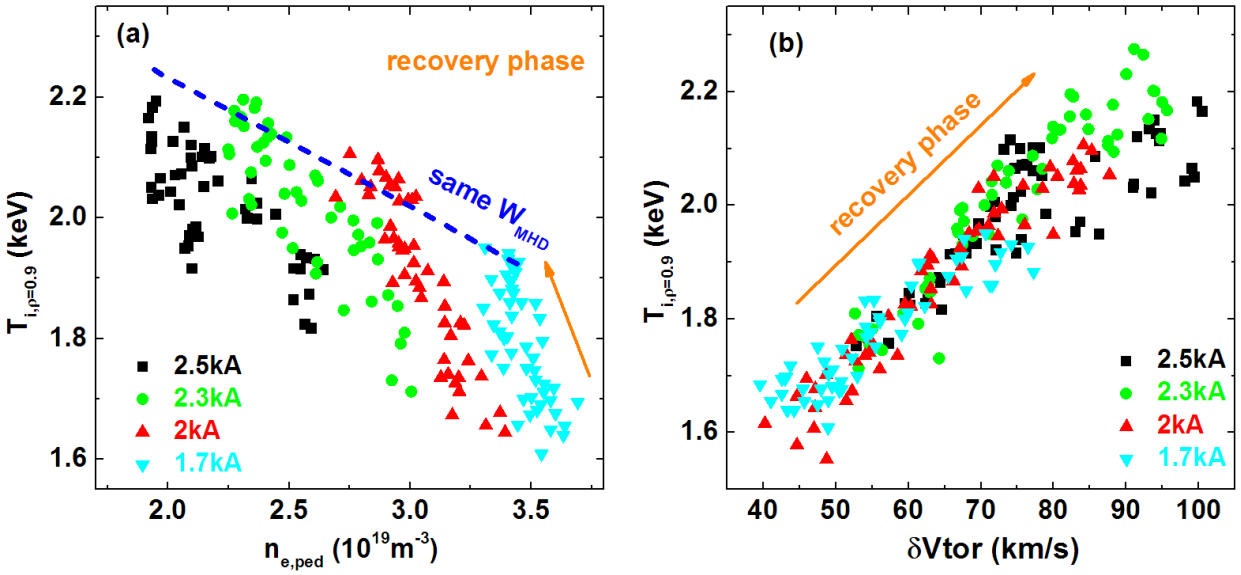

Figure 12 (a) Correlation between pedestal electron density and $T_{i,\rho=0.9}$. (b) Correlation between the difference of two edge toroidal rotation velocity dV_{tor} and $T_{i,\rho=0.9}$. Each data point comes from the time evolution at the recovery phase for four discharges #157381, #157378, #157377and #157372; with I-coil current 1.7kA, 2kA, 2.3 kA and 2.5kA respectively.

III. Transport modeling

In this section we use the TRANSP code to better understand the confinement response of the plasma to the RMP application in terms of the thermal electron and ion confinement. TRANSP is a time-dependent code used for power, particle and momentum balance calculations [5]. Given time-dependent plasma profiles, TRANSP solves the magnetic diffusion equations, electron and ion energy balances, particle balances, and neutral transport. It gives as outputs the energy and particle confinement times, thermal and particle diffusivities, as well as total pressure and calculated neutron rates which can be compared to the experiments [11]. From Fig. 13, we can see that TRANSP analysis produces good overall agreement with the measured neutron rate as well as the magnetic measurement of the total stored energy, indicating that the profile analysis and fast-ion content from NUBEAM [12] is consistent with the experiment, and there is no need to invoke anomalous fast-ion losses to reconstruct the plasma dynamics. In Fig. 13(b) we plot

the thermal and beam ion stored energy respectively, which show that the dominant confinement recovery is due to the thermal plasma energy, not the well-confined beam ion population. Only 20% of the stored energy increase in the recovery phase comes from the beam ions whereas the thermal plasma contributed the remaining 80% of the recovery from 2.4 to 2.8 s in shot#157378. In order to identify where the increment of thermal energy comes from, we plot the energy stored in the pedestal W_{ped} and core W_{core} to ions and electrons, where Fig. 14 shows the definition of W_{core} and W_{ped} from energy density profile, which is equivalent to pressure with a factor of 1.5. In Fig. 15 we separate the total thermal energy into ions [Fig. 15(a)] and electrons [Fig. 15(b)] and identify the pedestal (blue) and core contributions (red) to the total thermal ion/electron energy (black). We can see that the confinement improvement comes mostly from the ion thermal channel as indicated from the profiles in Fig. 7. It is interesting that W_{ped} for the ions is only increasing by ~ 5% over the recovery interval from t=2.4 to 3 sec, while the core ion stored energy ($W_{i,core}$) increases by 25%. The reason for this difference is that the edge density continues to decrease through the recovery phase, thus offsetting the increase from the edge ion temperature. From Fig. 15(b) we see that the $W_{e,ped}$ for the electrons decreases on the longer time scale arising from the continued fall of the electron density and the weak increase in the edge electron temperature. There is some thermal stored energy recovery for the electrons that is mostly offset by the continued fall in the $W_{e,ped}$. From these figures it can be seen that almost all of the confinement recovery comes from the improvement in the core ion thermal energy and this in turn is correlated with the increase in the edge Ti as discussed earlier.

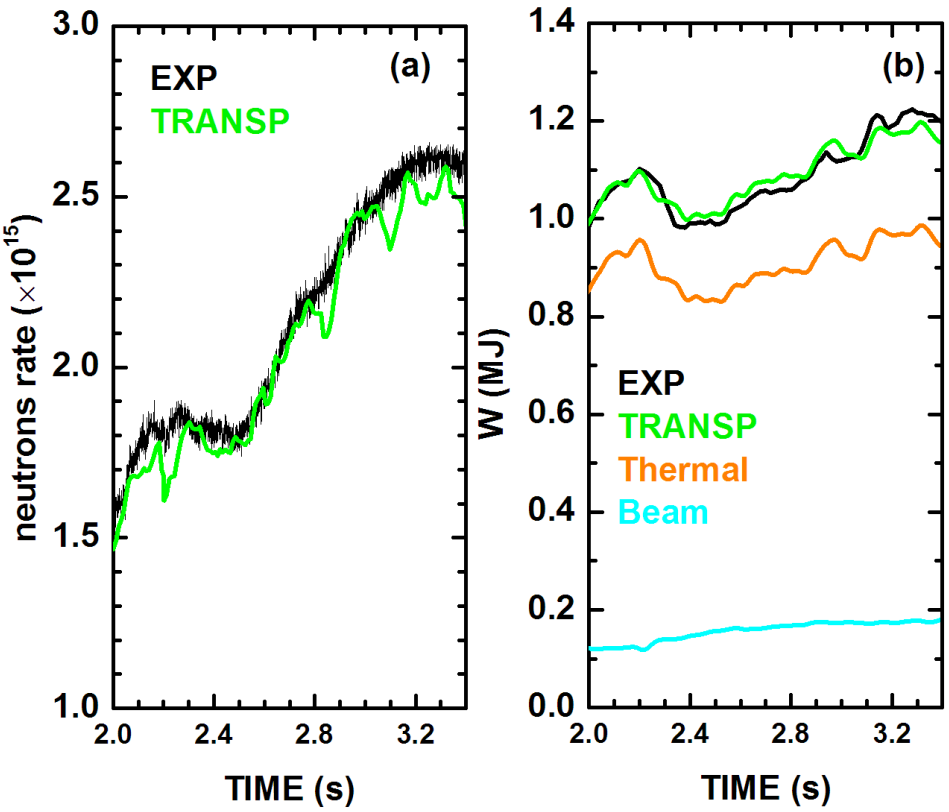

Figure 13 (a) TRANSP calculations of the total neutrons rate (shown in green) in comparison to measured neutrons rate (shown in black). (b) Experimental stored energy from magnetic (black), TRANSP calculation of the total stored energy (green), thermal (orange) and fast ion stored energy (blue) as a function of time.

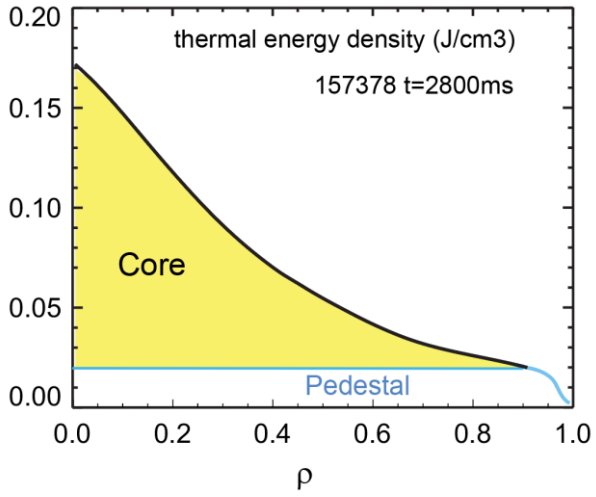

Figure 14 Illustration of $\mathbf{W_{core}}$ and $\mathbf{W_{ped}}$ from energy density profile.

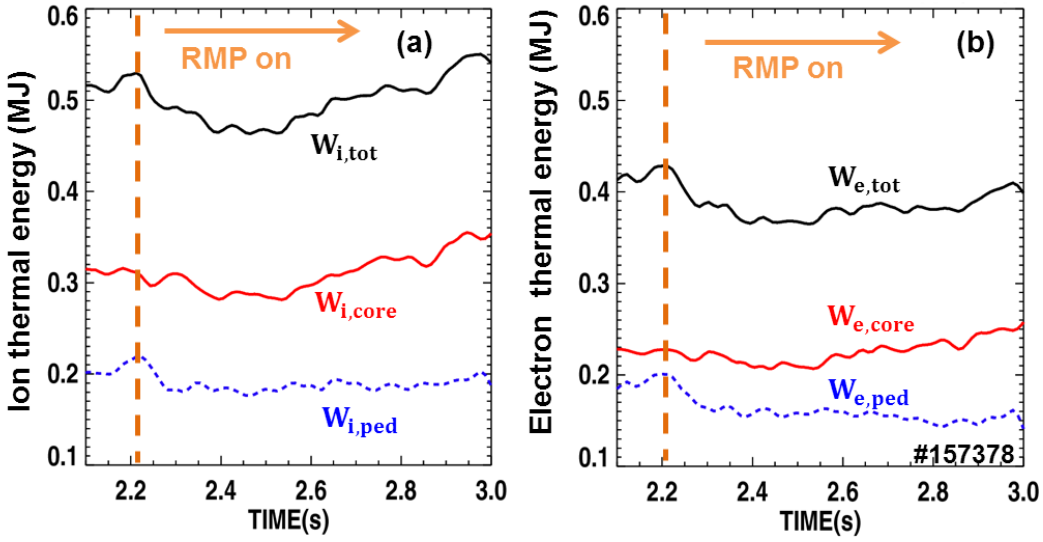

Figure 15 Thermal stored energy shown in different components of the pedestal and core for (a) ions and (b) electrons for shot # 157378.

To better understand the experimental observations, we employ the trapped-gyro-Landau-fluid (TGLF) model [13] in TRANSP to predict the core confinement improvement based on the evolution of pedestal parameters. The TGLF (trapped gyro-Landau fluid) model is a reduced transport model based on GYRO simulations [13-15]. It has been implemented in the TRANSP code to predict the core T_i profile using the

measured density and electron temperature profiles and $E \times B$ shearing rate derived from experimental measurements, and taking the ion temperature at ρ =0.8 as the boundary condition for the calculation. The results are shown in Fig. 16 for the two cases where (a) the T_i at ρ =0.8 is allowed to evolve as in the experiment, and (b) where T_i at ρ = 0.8 is held fixed at its initial value at the start of the recovery phase. From Fig. 16(a), we see that the predictive TRANSP run using TGLF obtains a good match to the measured T_i in the plasma core (here we show the T_i evolution at ρ at 0.4, 0.5 and 0.6), with the boundary condition for TGLF shown at ρ = 0.8. In order to isolate the effect of edge ion temperature on the core confinement, Fig. 16(b) shows the simulation where we kept all the other quantities the same but held the value of T_i at ρ =0.8 fixed from 2.4s onward. In this case, we see a much weaker increase in the core ion temperature compared to the simulation shown in Fig. 16(a). The strong correlation of the core and edge T_i observed in the experiment is therefore consistent with the predictions of ITG transport that leads to self-similar ion temperature profiles in the core of fusion plasmas. In Fig. 17 we show the TGLF prediction of the a/L_{Ti} at ρ = 0.4 compared to the experimental value at several time slices, showing the accuracy of the TGLF prediction.

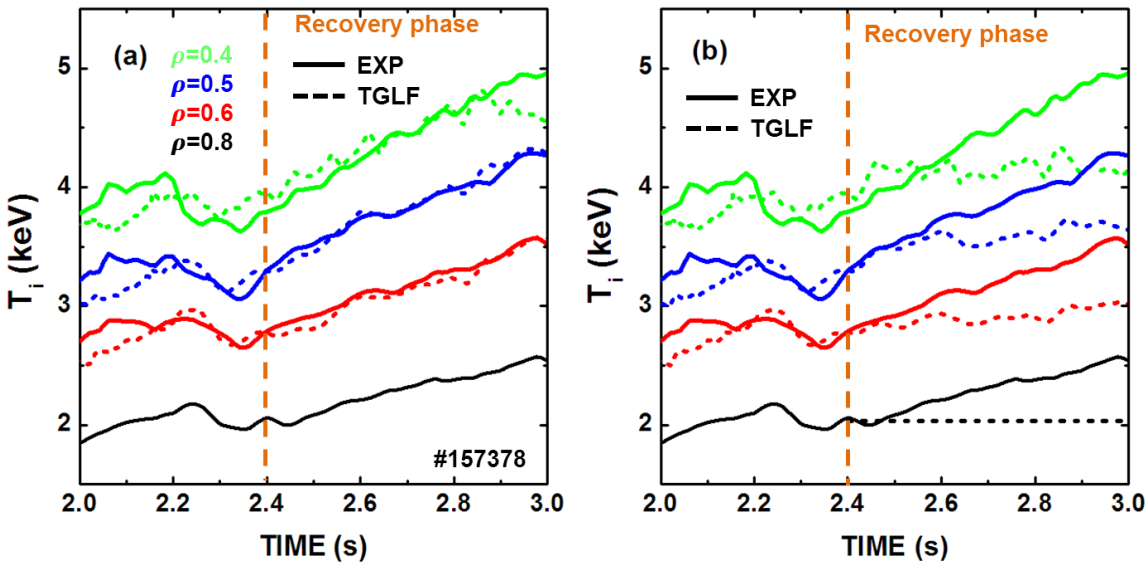

Figure 16 Comparison of time evolution of ion temperature at different $\boldsymbol{\rho}$ (0.4, 0.5, 0.6 and 0.8) for experiment (solid lines) and TRANSP/TGLF prediction (dash lines): (a) Using experimental $\boldsymbol{T_i}$ values at $\boldsymbol{\rho}$ =0.8 as TGLF boundary condition; (b) Using fixed edge experimental $\boldsymbol{T_i}$ at t=2.4s for all time for shot 157378.

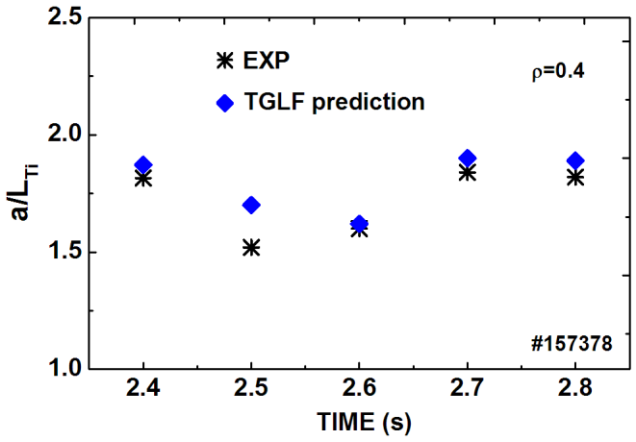

Figure 17 Comparison between experimental $\boldsymbol{a/L_{Ti}}$ and TGLF prediction at $\boldsymbol{\rho}$ = 0.4.

To further investigate the underlying physics of the core confinement improvement, we employed the transport simulation tool T-GYRO [16] that incorporates the neoclassical transport code (NEO) [17] and reduced turbulent transport code TGLF [13] to calculate the total ion thermal flux comprising of the sum of neoclassical and turbulent fluxes. By varying the inverse thermal ion temperature scale length (a/L_{Ti})

at specified radii, we obtain the corresponding ion energy flux predicted by T-GYRO. In Fig. 18 we show the result of such a scan at ρ = 0.4 with profiles taken at t = 2.8 sec in shot 157378. The ion energy flux shown in Fig.18 is normalized by the gyro-Bohm flux (Q = Q_{ion}/Q_{gB}, where $Q_{gB} = n_e C_s T_e (\rho_s/a)^2$ where a is the minor radius and C_s is the sound speed at the reference radius). At ρ = 0.4 and t=2.8 s TGYRO predicts strong transport stiffness at the experimentally relevant ion energy flux. This is consistent with our understanding that the core ion temperature increases in response to the increase in the edge ion temperature due to transport stiffness in the plasma core. In this case the measured inverse ion temperature scale length is within 10% of the theoretical prediction.

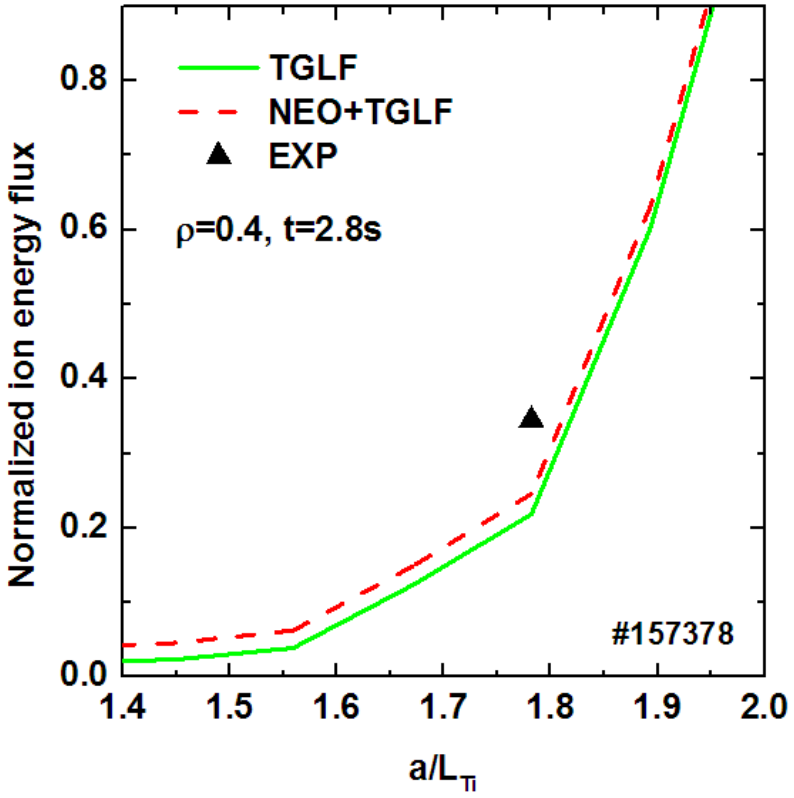

Figure 18 NEO + TGLF predicted flux verses a range of $\boldsymbol{a/L_{Ti}}$ for $\boldsymbol{\rho}$ = 0.4 at t = 2.8 s.

IV. Effect of Large RMP Amplitude on Confinement

We have shown that for low I-coil current up to the threshold of ELM suppression, improvement of confinement can occur due to the increase in the pedestal T_i and this increase is correlated with the reduction in the pedestal density and the increase in the edge ion temperature. At higher I-coil current a confinement recovery is seldom seen. In Fig. 19 we display the time evolution of plasma stored energy, electron density at ρ=0.9 and T_i vs T_e at ρ =0.9 for shot 157376 with 5 kA I-coil current corresponding to $\delta b_r^{(10,3)} B_T^{-1} \approx 4.4 \times 10^{-4}$ and constant beam power and torque. There is a much larger reduction in the stored energy (~ 43%) and pedestal density (~50%) in response to the 5 kA I-coil current as compared with shot 157372 with 2.5 kA I–coil current in Fig. 4. In the late RMP phase, there is also no strong recovery of the stored energy. In Fig. 19 (c), both the edge T_i and T_e decrease strongly with the application of the RMP in contrast to the cases with lower I-coil current. Although in the late RMP phase (t > 4.2 sec) there is an increase in both the edge T_i and T_e, the edge T_i increases only back to its pre-RMP level that is not enough to compensate the store energy loss through density pump-out in comparison to the low RMP shown in Fig. 5(b). Therefore only a slight increase in the stored energy has been seen, which is not sufficient to fully recover from initial drop.

TRANSP analysis for 157376 is shown in Fig. 20 revealing the different components of the plasma stored energy. Comparing to Fig. 15 (I_{RMP}= 2kA), there is a significant reduction in the core stored energy W_{core} for the high RMP case during the density pump-out phase, while in the low RMP case the core stored energy is barely affected by the application of the RMP. This is a consequence of a global reduction in the plasma density (not just in the edge) and a suppression of the electron temperature and ion temperature. While the edge ion and electron temperatures increase on a long time scale, the increase in the total stored energy of ≈ 0.15 MJ is much less than the large reduction (≈ 0.55 MJ) in the stored energy. While the stored energy increase in the late phase of the 5 kA I-coil discharge is comparable to the 2 kA case (Fig. 15), the initial reduction in stored energy during the pump-out phase is much larger. The large reduction of the stored energy at high I-coil current will be studied in a future work.

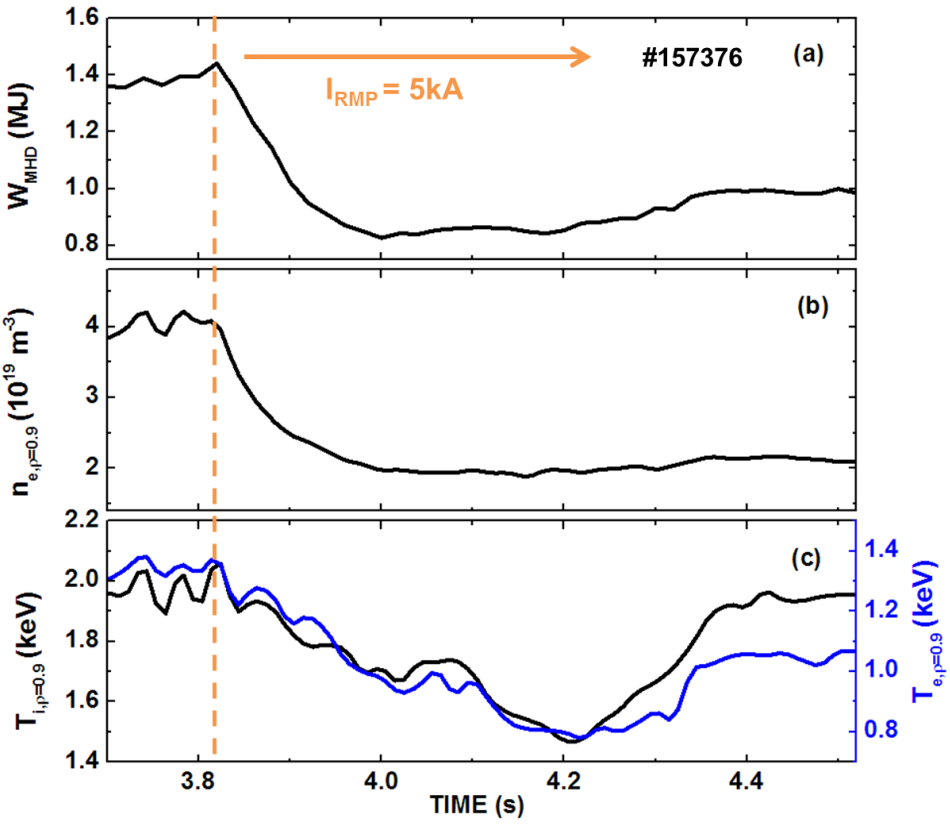

Figure 19 High RMP I-coil current condition (I_{RMP}=5kA) for shot 157376: (a) plasma stored energy, (b) electron density at ρ=0.9 and (c) ion temperature (black) and electron temperature (blue) at ρ ~ 0.9.

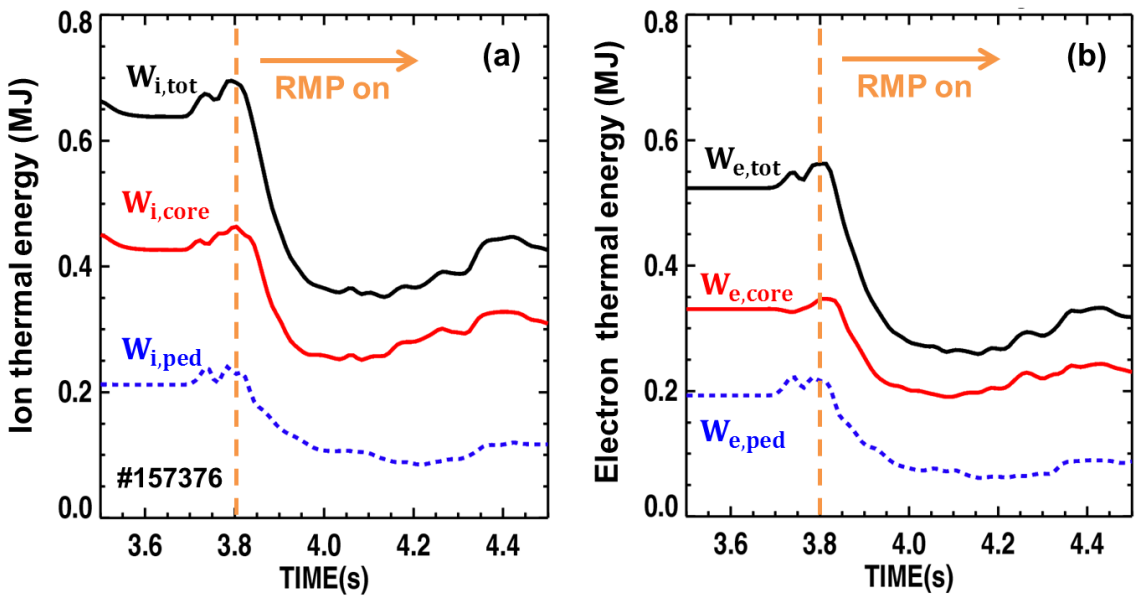

Figure 20 For shot 157376: thermal stored energy shown in different components of the pedestal and core for (a) ions and (b) electrons.

V Conclusions

In this paper we have shown that for modest RMP amplitudes near the threshold of ELM suppression the confinement experiences a long time scale recovery that often completely compensates for the initial degradation in confinement during density pump-out. The confinement degradation during pump-out is proportional to the change in the line average density while the ion and electron temperature profiles experience little change. However on a long time scale the ion temperature increases across the plasma radius. The increase in the ion temperature at the plasma edge is correlated with an increase in a/L_{Ti} and the E × B shearing rate at the top of the H-mode pedestal. From stability analysis using TGLF we find that the E × B shearing rate and the ITG linear growth rate are comparable at the top of the pedestal and increase together. These results are consistent with the improvement of the ion thermal confinement resulting from E × B shear induced reduction of turbulent transport at the top of the pedestal following density pump-out. In Fig.9, we plotted the different components of E × B shearing rate at pedestal top and it shows that it is the toroidal rotation gradient contributes most to the increase of E × B shearing rate.

One possible reason for the spins-up of edge toroidal rotation is the density reduction after the application of RMP, therefore the edge rotation increases according to the conservation of momentum. This is one of the possible origins of the increased E × B shear. However, the details of the mechanism need further investigation. The rise of the core ion stored energy is consistent with TGLF predictions of profile self-similarity based on the observed increase in the edge ion temperature. It is found that the increase in the ion confinement is correlated with the density pump-out induced by the RMP, and we notice that the recovery of the stored energy is only due to a noted increase in the edge ion temperature and not involved with an increase in the density. However we cannot speculate at this time on the relationship between the edge density reduction and the increase in the edge T_i.

At large RMP amplitude, the trend of the confinement recovery is to some extent similar to the low RMP cases that both are associated with the increase of edge ion temperature. However the major difference is in the much larger reduction of the stored energy with less recovery in the core ion thermal energy for the high RMP cases. This large (~40%) reduction in the stored energy results from both a large fraction of density reduction (~50%) as well as a significant drop in the edge temperature. The large drop in the plasma density with the higher I-coil current and the additional reduction in the edge ion and electron temperature are not well understood. A possible explanation is that the self-similarity seems break down in the core for the high RMP cases so that the edge T_i is decoupled from the core T_i. The reason why the self-similarity breaks down might be related to the larger NTV torque at high RMP amplitude that takes effect on the edge transport or E × B shearing. One path for future studies is to address the effect of the RMP induced NTV torque on transport and confinement.

A fundamental question arising from this study is why the edge T_i increases after density pump-out. Unfortunately this question is difficult to answer because we do not have a good transport model for the H-mode pedestal. However, it is important to recognize that the ion and electron temperatures can decouple at low density due to reduced collisionality. Therefore it will be interesting to explore the confinement effect of RMPs in higher density discharges maintaining ITER-like collisionality.

Acknowledgement

This work is supported by the U.S. Department of Energy under Awards No. DE-AC02-09CH11466，

DE-FC02- 04ER54698 and DE-FG02-05ER54809.

References

1. Loarte, A., et al., *Plasma density and temperature evolution following the H-mode transition at JET and implications for ITER.* Nuclear Fusion, 2013. **53**(8): p. 083031.

2. Evans, T.E., et al., *Edge stability and transport control with resonant magnetic perturbations in collisionless tokamak plasmas.* Nat Phys, 2006. **2**(6): p. 419-423.

3. Evans, T.E., et al., *RMP ELM suppression in DIII-D plasmas with ITER similar shapes and collisionalities.* Nuclear Fusion, 2008. **48**(2): p. 024002.

4. Grierson, B.A., et al., *Impurity confinement and transport in high confinement regimes without edge localized modes on DIII-Da).* Physics of Plasmas, 2015. **22**(5): p. 055901.

5. Hawryluk, R.J., *An empirical approach to Tokamak transport*. Commission of the European Communities (CEC). p. v119-46.

6. Jackson G.L. et al 2003 Proc. 30th EPS Conf. on Controlled Fusion and Plasma Physics (St Petersburg, Russia) CD-ROM P-4.47

7. Meneghini, O., et al., *Integrated modeling applications for tokamak experiments with OMFIT.* Nuclear Fusion, 2015. **55**(8): p. 083008.

8. Sun, H.J., et al., *Study of near scrape-off layer (SOL) temperature and density gradient lengths with Thomson scattering.* Plasma Physics and Controlled Fusion, 2015. **57**(12): p. 125011.

9. Waltz, R.E. and R.L. Miller, *Ion temperature gradient turbulence simulations and plasma flux surface shape.* Physics of Plasmas, 1999. **6**(11): p. 4265-4271.

10. Burrell, K.H., *Effects of E×B velocity shear and magnetic shear on turbulence and transport in magnetic confinement devices.* Physics of Plasmas, 1997. **4**(5): p. 1499-1518.

11. Greenwald, M., et al., *Energy Confinement of High-Density Pellet-Fueled Plasmas in the Alcator C Tokamak.* Physical Review Letters, 1984. **53**(4): p. 352-355.

12. Goldston, R.J., et al., *New techniques for calculating heat and particle source rates due to neutral beam injection in axisymmetric tokamaks.* Journal of Computational Physics, 1981. **43**(1): p. 61-78.

13. Staebler, G.M., J.E. Kinsey, and R.E. Waltz, *A theory-based transport model with comprehensive physicsa).* Physics of Plasmas, 2007. **14**(5): p. 055909.

14. Kinsey, J.E., et al., *ITER predictions using the GYRO verified and experimentally validated trapped gyro-Landau fluid transport model.* Nuclear Fusion, 2011. **51**(8): p. 083001.

15. Kinsey, J.E., G.M. Staebler, and R.E. Waltz, *The first transport code simulations using the trapped gyro-Landau-fluid modela).* Physics of Plasmas, 2008. **15**(5): p. 055908.

16. Candy, J., et al., *Tokamak profile prediction using direct gyrokinetic and neoclassical simulation.* Physics of Plasmas, 2009. **16**(6): p. 060704.

17. Belli, E.A. and J. Candy, *Kinetic calculation of neoclassical transport including self-consistent electron and impurity dynamics.* Plasma Physics and Controlled Fusion, 2008. **50**(9): p. 095010.